The Effect of Tuned Compensation Capacitors in the Induction Motors

MATHEW HABYARIMANA, GULSHAN SHARMA, PITSHOU NTAMBU BOKORO
Department of Electrical and Electronic Engineering Technology,
University of Johannesburg,
Doornfontein Campus,
SOUTH AFRICA

Abstract: - The load switch-on surge current phenomenon is a key problem for remote loads generally connected to weak or stand-alone grids. This has been the main research topic in smart microgrids. A correlation exists between the motor load and the starting current since a motor usually needs a larger starting current to overcome inertia. Both the power needed to start the load and the higher reactive power demand during the starting procedure are at the origin of the increased current. The current decreases to the nominal value for the specific load gradually after the motor starts. This relationship is essential for figuring out the dimensions of electrical components and protecting the grid and motor from harm. Depending on the load, the switch-on surge current is greater than two to ten times the rated full load current. Energy storage systems can make up for the higher power needed to protect the load and the grid connection. It makes more sense to use tuned compensating capacitors to reduce the reactive power required to reduce the inrush current. The primary focus of this work is the selection, calculation, and switching of the capacitor bank for reactive power compensation. Following the previous research, in this paper, the smaller 2HP induction motor load is examined. The capacitances are calculated, turned on to offset the starting transient, and then disengaged once the machine reaches operating speed. This is done by using a point-on switching technique that lowers the switching transient.

Key-Words: - Point on switching, Capacitor bank, micro-controller, Compensation.

1 Introduction

Large loads' inrush currents in power systems can result in issues with excessive current drawn and, in the case of weak grids, can destroy both the system equipment and the system network. Additionally, it may inadvertently set off protective relays, causing voltage drops that impair the functionality of additional devices connected to the same system. The goal of this research is to use capacitor switching to reduce inrush current.

Three-phase induction machines can be started in various ways to handle peak current and pulsing torques during the startup phase. For the machine's electrical protection unit, mechanical gearing systems, and electrical suppliers, this kind of performance is highly undesirable.

When a motor is connected to a power source that isn't strong enough, the abrupt increase in current leads in a temporary drop in voltage throughout the entire power bus, which powers the starting motor, [1]. In this study, a model for reducing inrush current on a power-rated induction motors in remote locations from the main grid and standalone microgrids is presented.

2 Literature Review

The issue of protection relays tripping unnecessarily or falsely is what sparked interest in the study of inrush current phenomenon, [2], [3], [4]. Five fundamental techniques were employed to start induction motors, [5], [6]. Excepting the direct online (DOL) starting, a starting method's primary goal is to lower the motor's supply voltage to lower the inrush currents specifically during the starting process. This is due to the supply voltage that directly impacts the starting currents.

However, there are advantages and trade-offs in terms of performance for every approach; When they first start, they all use the grid frequency.

Fig. 1: Three phase Induction Motor name plate

Modern starting techniques such as part winding arrangement and adjustable frequency drive (AFD) have been developed and some drawbacks were investigated in [5] and [7].

Based on the overall power system restrictions and the drive equipment, this study develops a way to minimize the starting current without requiring more motor design at a fair cost. Reactive power consumption is high in induction motors because they often have a relatively low power factor when they initially start. In the previous study the motor that was investigated in the experiments 5HP was bigger than the current one 2HP, to show the experimental results based on sizes.

The purpose of adding the capacitors in the motor control circuit is to enable it to function as generators of reactive power. The calculation of the initial peak of inrush current was the main task of early approaches (Table 1), [8], [9]. As previously used for the 5HP motor, in this research's suggested approach makes use of microcontroller programming with an algorithm written so that the network's capacitors are switched on whenever the current exceeds a predetermined value, "X," for the 2HP induction motor which represents both the inrush current and the starting period, which can also be determined by a low power factor (1).

$$\cos \theta = \frac{P}{VI\sqrt{3}} = \cos(\theta_v - \theta_i) \qquad (1)$$

Where θ_v and θ_i are are phase angles for voltage and current respectively, P is the total input power, I is the input line current, and V is the line voltage.

Depending on the steady-state conditions, the current decreases to the specified value or less once the motor reaches the rated speed. Since the capacitors no longer provide the reactive power compensation during starting, they can be carefully replaced. This will prevent the motor from entering a generator mode, which could seriously damage it due to the magnetizing current the capacitors

provide and the voltage at the motor terminals rising to nearly 50% of the rated voltage, [10], [11].

The next section discusses the point-on switching of the capacitors.

Fig. 2: Stator connection layout
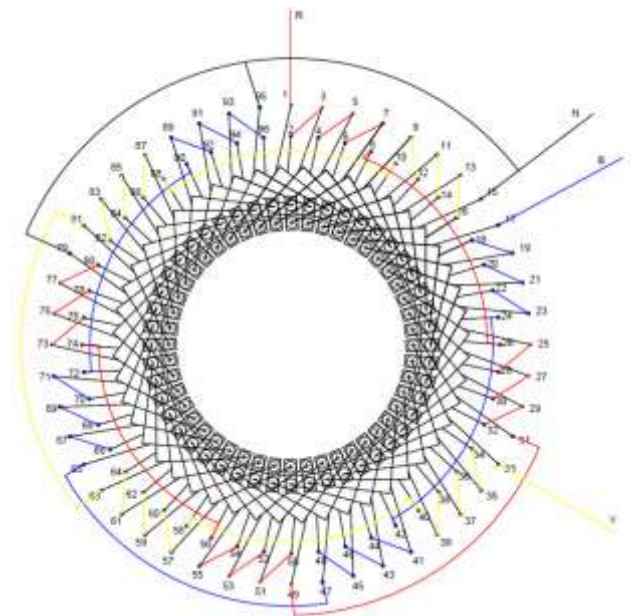
Fig. 3: Stator connection diagram

3 Motor Testing

The 50 Hz, 4 poles, 2hp, 3 Phase Induction motor used in this research has been tested to get the practical parameters used in the capacitor sizing and switching. Figure 1 shows the nameplate of it.

The instruments that are required are shown in Table 2. The synchronous speed and the Coil span (full pitch) are respectively given by (2) & (3).

$$Coil\ span = \frac{48}{4} = 12\ slots \qquad (2)$$

$$N = \frac{12f}{p} = \frac{120 \times 50}{4} = 1500\ rpm \qquad (3)$$

Table 1. The Various Starting Methods and Characteristics, [10]

	DOL	Auto Trans-former	Solid State Starters	Adjustable Freq. Drives	Primary Resistor / Reactor	Part Winding	Wye Delta
Initial System Cost	Low	Moderate	Higher	Highest	Moderate	Low	Low
Starting Current	Highest	Low	Moderate	Lowest	Moderate	Moderate	Low
Starting Torque	Highest	Low	Low	Highest	Low	Low	Low

Table 2. Required Instruments

S. No.	Name	Range	Qty
1	Ammeter	5A	1
2	Voltmeter	0-500	1
3	Wattmete	5/10A, 150/300/600V	2
4	3 phase Variac	6A	1

Table 3. Coils Inter Connection Terminal Coding

Phase A	Phase B	Phase C
1 (Input Terminal Point)	**17 (Input Terminal Point)**	**33 (Input Terminal Point)**
2-3	18-19	34-35
4-5	20-21	36-37
6-7	22-23	38-39
8-26	24-42	40-58
25-28	41-44	57-60
27-30	43-46	59-62
29-32	45-48	61-64
31-49	47-65	63-81
50-51	66-67	82-83
52-53	68-69	84-85
54-55	70-71	86-87
56-74	72-90	88-10
73-76	89-92	9-12
75-78	91-94	11-14
77-80	93 -96	13-16
79 (Neutral point)	**95 (Neutral point)**	**15 (Neutral point)**

Table 4. Equivalent Circuit Parameters

Description	Data source	Symbol	Value
Stator resistance	Measured	R1	2.3 Ω
Stator reactance	Calculated	X1	3.39 Ω
Stator inductance	Calculated	Lls	5.262mH
Rotor resistance	Calculated	R2	3.13 Ω
Rotor reactance	Calculated	X2	7.91 Ω
Rotor Inductance	Calculated	L1r	5.262mH
Core resistance	Measured	RC	222.78 Ω
Magnetizing reactance	Calculated	Xm	95.48 Ω
Magnetizing inductance	Calculated	Lm	178.91mH
Number of poles	Number plate	P	4 poles
Rated stator voltage	Number plate	V rated	220 V
Rated rotor speed	Number plate	N rated	1485 rpm
Supply frequency	Number plate	f	50 Hz
Inertia constant	Calculated	j	0.012
Total Number of stator coils per phase	counted	Ns	16

Table 5. No Load Motor Test Results

Measurement Value	Value
Line to line voltage, VL-L	220 V
Line current, IL	2.7 A
Rotor speed	1484 rpm
Supply frequency	50 Hz
Stator resistance, R1	2.1293 Ω
Three phase power with 2 Wattmeters	W1,nl = 90x2=180W W2,nl = 83x5=415W Pnl = 595W
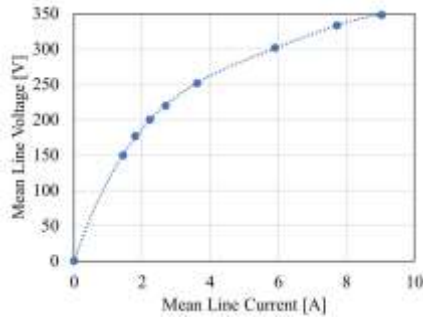
Fig. 4: Running light test - variation of current with voltage
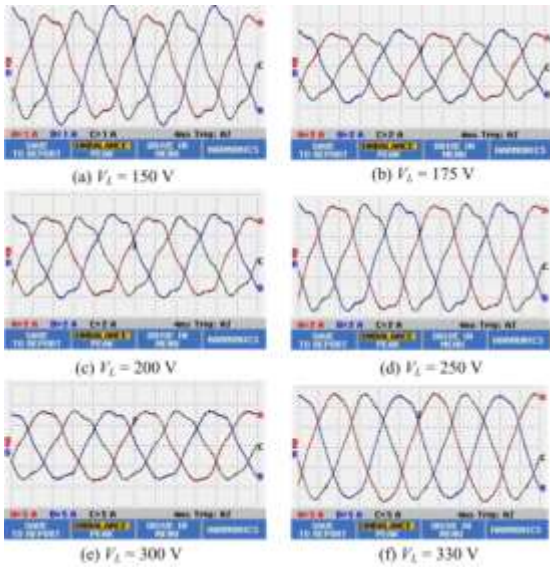
Fig. 5: Running light test current waveforms

This is a four-pole connection, meaning that each pole's coils are connected in series with the poles themselves. Figure 3 & Figure 2 displays the Stator connection diagram and configuration.

The machine specification from the nameplate is summarized as follows:
• Nominal Current: 3.7 Amperes per terminal
• Nominal voltages: 380 Volts
• Nominal Power: 2 Horse Power (1.5kW)
• Rated speed: 1400 rpm
• Network frequency: 50 Hz
• power factor 0.79
• efficiency 78.5%

Table 4 shows the equivalent of circuit parameters measured and or counted during the experiment.

3.1 Running Light Test

The Measured no-load values from the test are shown in (Table 5).

The equivalent circuit parameters are summarised in Table 3.

The core loss, magnetizing reactance, were calculated as (4) and (5).

$$P_{rot} = P_n - R_s I_n^2 = 595 - 2.1293 \times 2.7^2 = 579.4774 \ W \qquad (4)$$

$$R_c = \frac{V_{ph}^2}{P_{ph}^2} = \frac{\left(220/\sqrt{3}\right)^2}{595/3} = 81.3445\Omega \qquad (5)$$
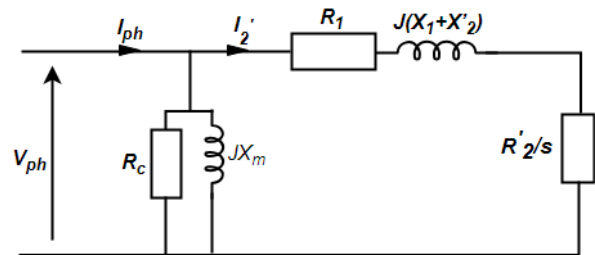
Fig. 6: Rotor loop

Table 6. Locked Rotor Test Results

V$_{13[V]}$	V$_{21[V]}$	V$_{32[V]}$	I$_{Linemean[V]}$	I$_{1[A]}$	I$_{2[A]}$	I$_{3[A]}$	I$_{Linemean[A]}$
160.5	147.8	150.3	152.87	1.44	1.44	1.44	1.44
175.5	178.8	176.3	176.87	1.78	1.96	1.64	1.79
200.3	198.6	200.8	199.9	2.19	2.4	2.09	2.23
220.1	218.3	220.6	219.67	2.69	2.85	2.51	2.68
252.3	250	252.2	251.5	3.68	3.77	3.39	3.61
302.3	300.1	302.2	301.53	6.02	6.06	5.63	5.9
332.9	332.9	332.9	332.9	7.8	7.84	7.51	7.72
350.2	347	347.5	348.23	9.19	9.19	8.73	9.04

Table 7. Locked Rotor Test Measurements

Line to line voltage	V$_{bl,L-L}$	46 V
Line current	I$_L$	5.8 A
Supply frequency	f	50 Hz
Stator resistance	R$_1$	1.5244 Ω
Three phase power, 2 Wattmeters	P$_{nl}$	W$_{1,nl}$ = 90x2=180W
		W$_{2,nl}$ = 83x5=415W
		W$_1$ +W$_2$= 595W

$$Q_{ph} = \sqrt{(V_{ph}I_{ph})^2 - P_{ph}^2} =$$

$$\sqrt{\left(\frac{220}{\sqrt{3}} \times 2.7\right)^2 - \left(\frac{595}{3}\right)^2} = 279.7783 \text{VAr}$$

$$(6)$$

$$X_m = \frac{V_{ph}^2}{Q_{ph}} = \frac{\left(\frac{220}{\sqrt{3}}\right)^2}{279.7783} = 57.6647\Omega \qquad (7)$$

The power factor is given by (8)

$$cos\,\phi = \frac{P_{nl,ph}}{U \times I_{nl}} = \frac{595/3}{220/\sqrt{3} \times 2.7} = 0.5783 \quad (8)$$

$$\phi = 54.6674°$$

$$Im = In\,sin\,\phi = 2.7\,sin\,54.6674° = 2.2027\,A$$

$$Ic = Inl\,cos\,\phi = 2.7\,cos\,54.6674° = 1.5615\,A$$
$$(9)$$

$$L_m = \frac{V_{n,pn}}{2\pi f_5 I_m} = \frac{220/\sqrt{3}}{2\pi \times 50 \times 2.2027} = 0.3179H$$

The no load impedance per phase (10):

$$Z_{nl} = \frac{V_{ph,n}}{I_{nl}} = \frac{220/\sqrt{3}}{2.7} = 47.0434\Omega \qquad (10)$$

The No load resistance per phase (11):

$$R_{nl} = \frac{P_{nl}}{3I_{nl}^2} = \frac{595}{3 \times 2.7^2} = 27.2062\Omega \qquad (11)$$

The No-load reactance per phase is (12):

$$X_{nl} = \sqrt{Z_{nl}^2 - R_{nl}^2} = \sqrt{47.0434^2 - 27.2062^2} =$$
$$38.3784\Omega \qquad (12)$$

The IV curve for the no load test is show on Figure 4.

As seen in Figure 5, the current wave-forms were also examined. Because of the short-pitched winding and saturation, these exhibit some distortion.

3.2 Locked Rotor Test

This test is conducted at a much-reduced voltage with a rated full-load current and with the rotor firmly locked so that it does not rotate.

The machine is supplied by an auto-transformer so that the voltage can be increased slowly. For this test, the current flowing through the magnetizing components is assumed to be negligible since the voltage is so much reduced (perhaps only 10 % of the rated voltage). In this case, we can assume that all the current is flowing through the rotor loop (Figure 6) and the results are shown in Table 6 and Table 7.

The power is measured with the 2-wattmeter method, each wattmeter with the multiplying factor. The no-load impedance per phase (13):

$$Z_{bl} = \frac{V_{bl,ph}}{I_{bl}} = \frac{46/\sqrt{3}}{5.8} = 4.579\Omega \qquad (13)$$

The stator + rotor resistance (14):

$$R_1 + R_2' = \frac{P_{ph,bl}}{3I_{bl}^2} = \frac{595}{3 \times 5.8^2} = 5.895\Omega \qquad (14)$$

Stator and rotor leakage reactance (15):

$$X_{is} = X_{ib}' = \frac{X_{bl}}{2} = \frac{5.0589}{2} = 2.5295\Omega \qquad (15)$$

The power factor (16):

$$cos\,\phi_{bl} = \frac{P_{bl,ph}}{U \times I} = \frac{645/3}{85/\sqrt{3} \times 8.2} = 0.5343 \quad (16)$$
$$\phi_{bl} = 57.7035°$$

4 Simulation Results

To achieve a complete conclusion for this research that started before, [12], [13], seven different induction machine properties have been examined, spanning a broad range of power, voltage, and pole number. The first was a laboratory motor (3) with four poles and 5 hP at 346 V. During the experiment, the machine's voltage was de-rated to 220 V.

The testing procedure and outcomes for the running-light and locked-rotor tests are shown in Table 5.
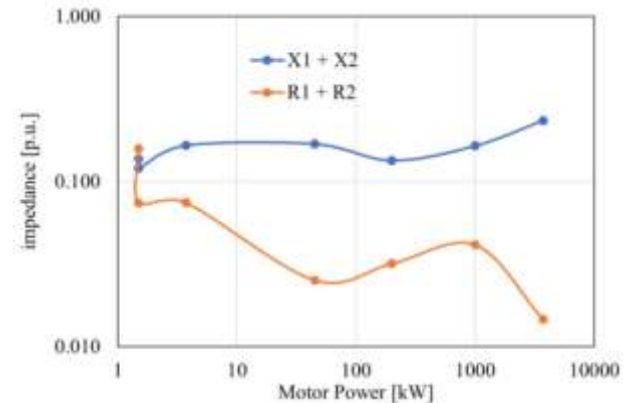
Fig. 7: P.U. input resistances and reactances at start for different motors
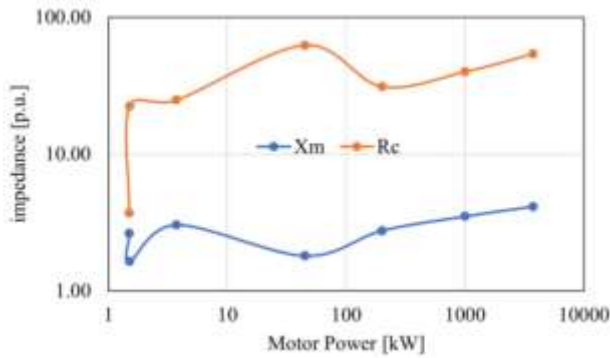
Fig. 8: Variation of P.U. Xm and Rc for different motors

Fig. 9: Power factor start for different motors.

The normalization is done using (17).

$$Z_{in}(1\,p.u.) = \frac{V_{Line\,(rated)}}{\sqrt{3}I_{Line(rated)}} \qquad (17)$$

Figure 8 shows the P.U. values for $R_1 + R_2'$ and $X_1 + X_2'$ plotted versus motor power. Be aware that the scale on both axis is logarithmic. As can be shown, $R_1 + R_2'$ fluctuates with a general trend downwards with increasing motor power, but

$X_1 + X_2'$ is largely constant across the spectrum, with the 1.5kW lab machine serving as an exception of Figure 9 plots Xm and Rc. The two axes are logarithmic once more.

With increasing power, the magnetizing reactance Xm shows a little increase trend but remains almost constant. The lab machine is an anomaly once more, with a much lower core loss resistance. The core loss resistance is significantly larger and follows the same rising pattern (Table 10).

The overall simulink model is shown in Figure 10 and Figure 11 shows the waveforms for lab Motor with $90\mu F$ Capacitors.

To compare with the laboratory machine, there is a 1.5 kW (2hP), 380 V, 4-pole, 50 Hz machine; a larger LV machine is represented by a 45 kW, 400 V, 4-pole, 50 Hz machine; an example of a higher-speed MV machine is a larger 2-pole, 200 kW, 3300 V machine; and an example of a larger MV low-speed motor is a 1 MW 6-pole, 6000 V.

The firm website, [14], included data sheets and test reports, including running-light and locked-rotor test results. Two example machines that [15], analyzed are included to add even more machines to the mix; these are examples of 60 Hz machines to provide variance. As an example of a very big MV machine, there is a modest 3.75 kW, 440 V, 4-pole, 60 Hz machine and a very huge 3.75 MW, 6900 V, 12-pole, 60 Hz machine. The parameters displayed by these machines are diverse and can be found in Table 8. The parameters were computed using data from running-light and locked rotor tests, or they were derived from manufacturer data sheets.

Table 9 contains the equivalent circuit parameters for each phase, either measured through testing or derived from the sources. The reactance resistance at startup is represented by the ratio X/R, and it is evident that larger machines are often significantly more inductive than smaller machines at this point. Figure 7 displays the initial power factors, which support the overall pattern of the power factor at start declining with increasing size. While the power range of the machines under study likely encompasses the entire range of 3-phase induction motors available, this is obviously largely dependent on the motor design. The power is on a logarithmic scale, as you can see.

5 Experimental Procedure and Calculations

The switching of capacitors is done following specific conditions and using the programmed microcontroller. This will reduce the inrush current. There are two types of capacitor connection; star (or Wye) and delta. In this research, the capacitor will be connected in delta. Star-connected capacitors for motors are not an appropriate connection and can potentially cause a failure to not only the capacitor but to the motor as well. For the star connection, capacitors are not grounded and can present a potential difference on each phase of the capacitor therefore contributing to the deterioration of the motor and capacitors connected.

Table 8. Motor Parameters

No.	Machine	kW	V Line [V]	I Line [A]	Poles	f_s [Hz]	rpm	J[kg.m²]
1	Lab machine	1.5	220	5.8	4	50	1425	0.0 12
2	Valiadas K90L-4	1.5	400	3.3	4	50	1440	
3	Sen 5 HP	3.75	440	3.73	4	60	1753	0.05
4	Yaliadis K200L-4	45	400	8 1. 1	4	50	1480	0.246
5	Valiadas KHV355-2	200	3300	44.4	2	50		2.6
6	Valiadas TMKHV560-6	1000	6000	110	6	50	990	79
7	Sen 5000 HP	3730	6900	358	12	60	596	145.47

Table 7. Motor Equivalent Circuit Parameters (Values in Ω)

No.	Machine	X_m	R_c	R_1	R_2'	$X_1 + X_2'$	XIR
1	Lab machine	58	81	2.13	1.34	2.99	0.86
2	Valiadas K90L-4	115.2	1568.2	1.325	3.87	8.44	1.62
3	Sen 5 HP	110	900	1.2	1.5	6	2.22
4	Valiadis K200L-4	5. 13	178.1	0.059	0.0 13	0.48	6.67
5	Valiadas KHV355-2	118	1333	0.79	0.57	5.75	4.2
6	Valiadas TMKHV560-6	102.5	900	0.97	0.24	4.78	3.97
7	Sen 5000 HP	46	600	0.083	0.08	2.6	15.95

Table 80. Motor Equivalent Circuit Parameters (Values in P.U.)

No.	Machine	Z_{in} 1 $p.u.$ [Ω]	X_m	R_2	R_1	R_2'	$X_1 + X_2'$
1	Lab machine	37.478	1.54	2.17	0.0568	0.0357	0.08
2	Yaliadas K90L-4	69.98	1.65	22.41	0.189	0.0554	0. 121
3	Sen 5 HP	36.29	3.03	24.8	0.0331	0.0413	0. 165
4	Yaliad is K200L-4	2.85	1.8	62.56	0.0207	0.0046	0. 169
5	Yaliadas KHY355-2	42.91	2.75	3 1.08	0.0184	0.0314	0. 134
6	Valiadas TMKHY560-6	29. 11	3.5	40	0.0332	0.0082	0. 164
7	Sen 5000 HP	11.1 3	4. 13	53.92	0.0075	0.0072	0.234
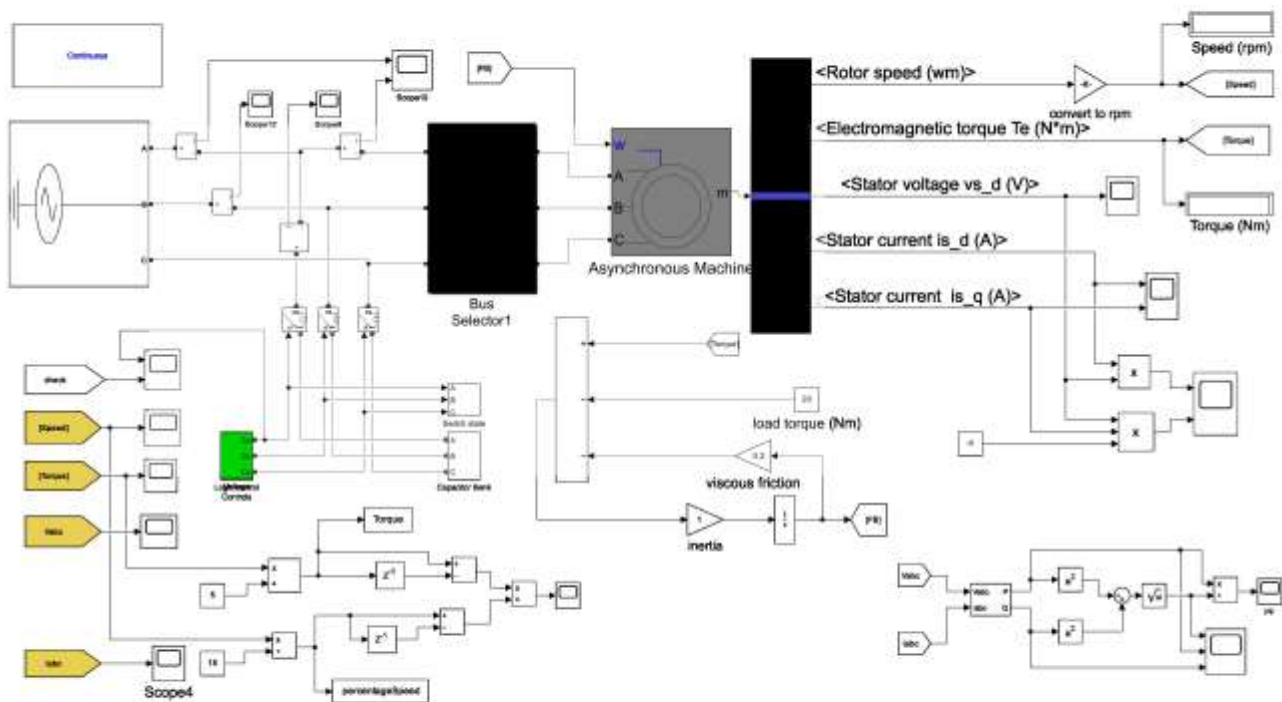
Fig. 10: Simulink mode
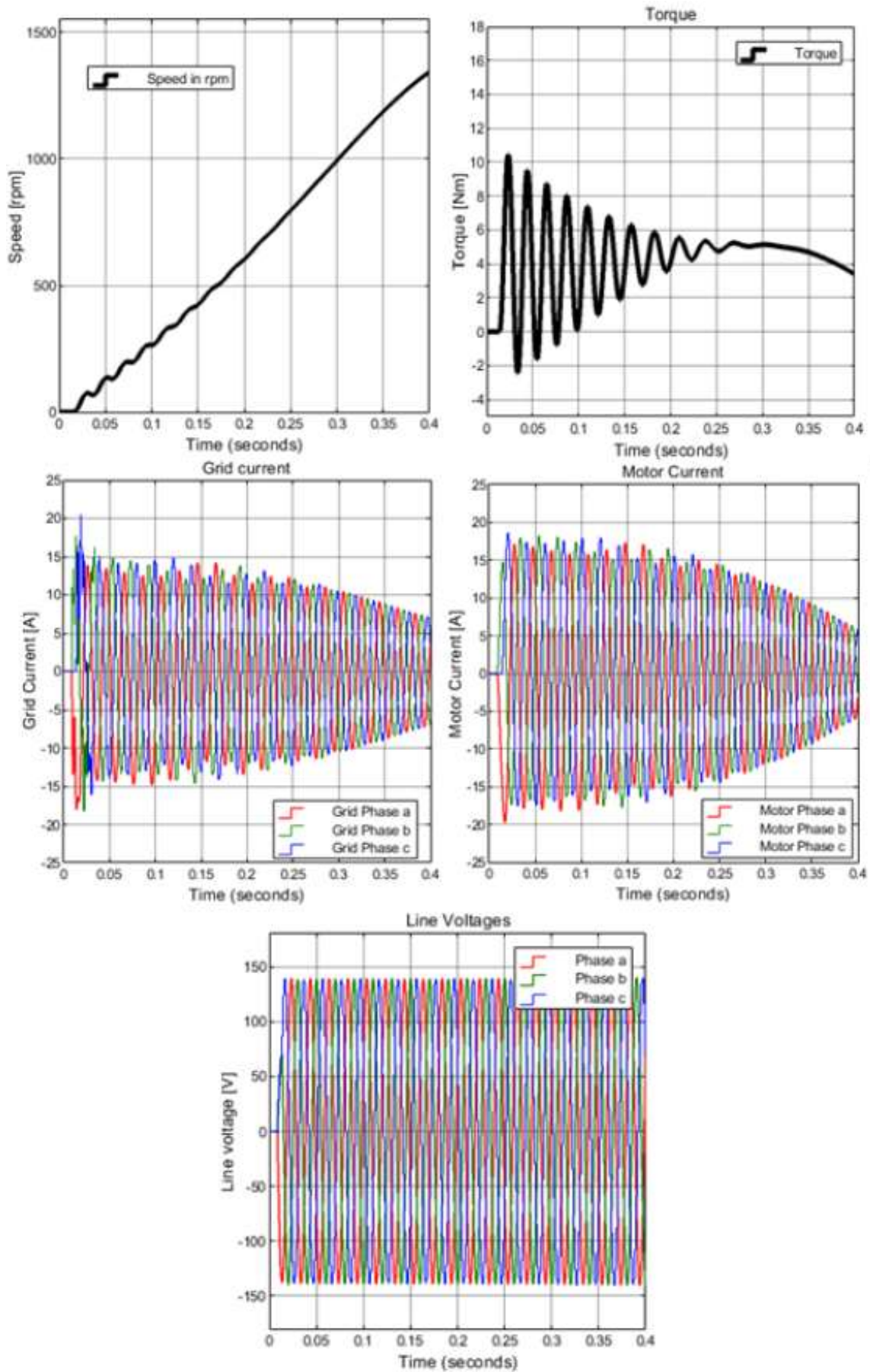
Fig. 11: Transient simulation of lab Motor with 90 μF capacitors

The failure of the capacitor causes motor breakdown because it makes the load unbalanced (Figure 13) therefore the motor is gets damaged following the unbalanced voltage and overheat which will eventually burn it out, [16]. Unprotected Star-connected capacitors should not be used for Power Factor correction for similar reasons. The protection of this type of connection is costlier than the capacitors themselves and, thus not generally included within the connection circuit. The overall layout of the test rig is shown in Figure 12.

Delta connection is the one chosen in this research. It does provide capacitance to each phase but does not provide voltage unbalance (harmonics), [17]. In the case of a failure of one capacitor cell for one phase for any reason, it moves from a closed delta to an open delta configuration. In this case, the voltage remains unchanged as shown in Figure 13. Figure 14 illustrates the capacitor connection model of a 3-phase induction motor used in this research; the capacitors C1, C2, and C3 are connected in delta. In the delta connection, capacitors are capable of circulating harmonic currents within the circuit, therefore reducing the harmonics of the electrical system.

The instantaneous voltage equations are written as (18):

$$v_a = v_m \cos(\omega t)$$
$$v_b = v_m \cos\left(\omega t - \frac{2\pi}{3}\right) \quad (18)$$
$$v_c = v_m \cos\left(\omega t - \frac{4\pi}{3}\right)$$

Assuming the three capacitors are equal size for a balanced

Motor $C_1 = C_2 = C_3 = C$, the current through each capacitor can be calculated from (19):

$$\begin{bmatrix} i_{C1} \\ i_{C2} \\ i_{C3} \end{bmatrix} = \frac{d}{dt} \begin{bmatrix} V_m \cos(\omega t) - V_m \cos\left(\omega t - \frac{2\pi}{3}\right) \\ V_m \cos\left(\omega t - \frac{2\pi}{3}\right) - V_m \cos\left(\omega t - \frac{4\pi}{3}\right) \\ V_m \cos\left(\omega t - \frac{4\pi}{3}\right) - V_m \cos(\omega t) \end{bmatrix} \quad (19)$$

The motor parameters need to be specified to calculate the time to connect the capacitors; in this simulation case we use the same as in [12], as shown in the equations (20).

$$X_c = \frac{3V_{ph}^2}{Q_{start}} = \frac{3 \times 100^2}{3500} = 31.1\Omega \quad (20)$$

And (21).

$$C = \frac{1}{2\pi \times 50 \times X_c} = \frac{1}{2\pi \times 50 \times 31.1} = 102\mu F \quad (21)$$

where X_c is the starting capacitive reactance, XQ_{start} is the starting reactive power, V_{PH} is the phase voltage, and C is the capacitance. The grid frequency is 50 Hz.

The maximum voltage V_m is given by (22)

$$v_m = v_{ph} = 220V \quad (22)$$

Therefore, capacitor currents iC are, for a 50 Hz system (23):
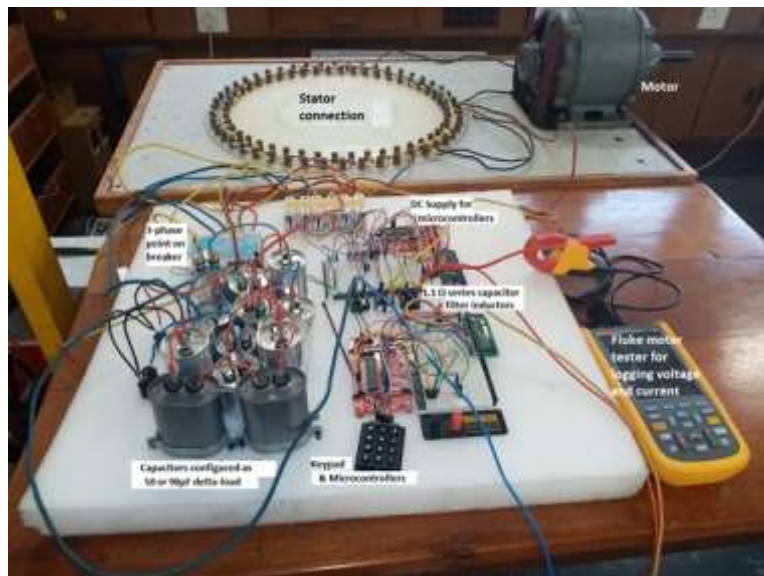
Fig. 12: Final layout of test rig
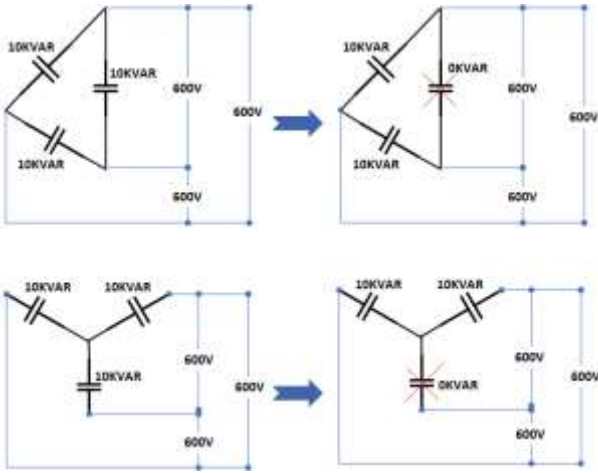
Fig. 13: The failure of any one cell of a Star and/or Delta connected
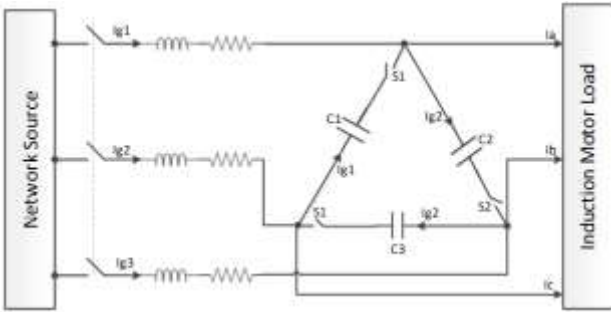
Fig. 14: Capacitor connection model to the load

$$\begin{bmatrix} i_{C1} \\ i_{C2} \\ i_{C3} \end{bmatrix} =$$

$$220 \frac{d}{dt} \begin{bmatrix} \cos(100\pi t) - \cos\left(100\pi t - \frac{2\pi}{3}\right) \\ \cos\left(100\pi t - \frac{2\pi}{3}\right) - \cos\left(100\pi t - \frac{4\pi}{3}\right) \\ \cos\left(100\pi t - \frac{4\pi}{3}\right) - \cos(100\pi t) \end{bmatrix} \times$$

$$[C] \tag{23}$$
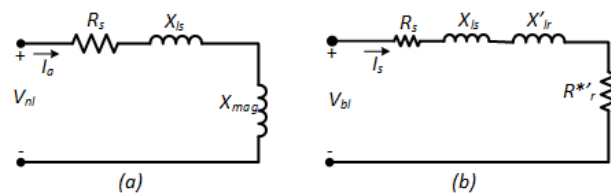
Fig. 15: Per phase equivalent circuit in the induction motor under the no-load

The motor size may vary but the main concept of capacitor switching remains the same.

The Machine 50 Hz, 4 poles, 2 hp, 3-phase Induction motor is also tested with a synchronous speed of 1500 rpm. Tests are done for parameter determination according to its equivalent circuit (Figure 15).

For the 4-pole connection, the coils in each pole are connected in series.

The magnetization reactance is calculated from (24).

$$X_m = \frac{V_{ph}^2}{Q_{ph}} = \frac{(220/\sqrt{3})^2}{279.78} = 57.67\Omega \tag{24}$$

The power factor is (25).

$$\cos\phi = \frac{P_{nl,ph}}{U \times I_{nl}} = \frac{595 \times \sqrt{3}}{220 \times 3 \times 2.7} = 0.5783 \tag{25}$$

so the angle is (26).

$$\phi = 54.67° \tag{26}$$

$$I_m = I_m \sin\phi = 2.7 \sin 54.67° = 2.20A \tag{27}$$

$$I_c = I_{nl} \cos\phi = 2.7 \cos 54.67° = 1.56A \tag{28}$$

$$L_m = \frac{V_{m,ph}}{2\pi f_s I_m} = \frac{220/\sqrt{3}}{2\pi \times 50 \times 2.2027} = 0.318H \tag{29}$$

The no-load impedance per phase (30):

$$Z_{nl} = \frac{V_{ph,in}}{I_{nl}} = \frac{220/\sqrt{3}}{2.7} = 47.04\Omega \tag{30}$$

No load resistance per phase (31):

$$R_{nl} = \frac{P_{nl}}{3I_{nl}^2} = \frac{595}{3 \times 2.7^2} = 27.21\Omega \tag{31}$$

$$X_{nl} = \sqrt{Z_{nl}^2 - R_{nl}^2} = \sqrt{47.0434^2 - 27.2062^2} =$$
$$38.38\Omega \tag{32}$$

The no load impedance per phase is given by (33):

$$Z_{bl} = \frac{V_{bl,ph}}{I_{bl}} = \frac{46/\sqrt{3}}{5.8} = 4.579\Omega \tag{33}$$

The stator + rotor resistance (34):

$$R_1 + R_2' = R_{bl} = \frac{P_{ph,bl}}{3I_{bl}^2} = \frac{350}{3 \times 5.8^2} = 3.468\Omega \tag{34}$$

No load reactance per phase (35):

$$X_{bl} = x_1 + x_2 = \sqrt{Z_{bl}^2 - R_{bl}^2} =$$
$$\sqrt{4.579^2 - 3.4681^2} = 2.99\Omega \tag{35}$$

It is assumed that $X_1 = X_2'$ then (36)

$$X_1 = X_2' = \frac{X_{br}}{2} = \frac{2.9899}{2} = 1.495\Omega \tag{36}$$

The stator winding (37 and 38) is obtained from a DC measurement between two phases, where $V_{dc} = 24.7$ V and $I_{dc} = 5.8$ A:

$$R_1 = \frac{1}{2} \times \frac{24.7}{5.8} = 2.13\Omega \qquad (37)$$

$$\cos\phi = \frac{P_{bl,ph}}{U_{bl} \times I_{bl}} = \frac{350/3}{46/\sqrt{3} \times 5.8} = 0.7574 \qquad (38)$$

The reactive power is given by (39):

$$Q_{ph} = \sqrt{(V_{ph}I_{ph})^2 - P_{ph}^2} =$$
$$\sqrt{(46/\sqrt{3} \times 5.8)^2 - (350/3)^2} = 100.58\text{Var} \quad (39)$$

where (40):

$$R_2 = Z_{bl}\cos\phi_{bl} - R_1 = 4.579 \times 0.7574 - 2.1293 \; 1.339 \,\Omega \qquad (40)$$

The magnetizing reactance is (41):

$$X_m = \frac{V_{bl,ph}^2}{Q_{Bl,ph}} = \frac{(46/\sqrt{3})^2}{100.5798} = 7.0127\Omega \qquad (41)$$

The air-gap power and starting torque are given by (42), (43) and (44):

$$P_{\text{gap}} = P_{br} - n_{ph}I_{br}^2 R_1 = 350 - 3 \times 5.8^2 \times 2.1293 = 135.1110\text{W} \qquad (42)$$

$$T_{\text{start}} = \frac{P_{\text{gap}}}{\omega_s} = \frac{135.1110}{155.4041} = 0.8694\text{N.m} \qquad (43)$$

$$T_{\text{mech}} = \frac{369.94}{157.08} = 2.3\text{N.m} \qquad (44)$$

By applying Kirchhoff's current law, the instantaneous input current i_g is given by (45):

$$\begin{bmatrix} i_{g1} \\ i_{g2} \\ i_{g3} \end{bmatrix} = \begin{bmatrix} i_a \\ i_b \\ i_c \end{bmatrix} + \begin{bmatrix} i_{c1} \\ i_{c2} \\ i_{c3} \end{bmatrix} - \begin{bmatrix} i_{c3} \\ i_{c1} \\ i_{c2} \end{bmatrix} \qquad (45)$$

With;

$$\begin{bmatrix} i_a(t) \\ i_b(t) \\ i_c(t) \end{bmatrix} = \begin{bmatrix} I_m\sin(\omega t) \\ I_m\sin(\omega t - 120) \\ I_m\sin(\omega t - 240) \end{bmatrix} \qquad (46)$$

(Angles to be converted in radians).
Considering the maximum current Im as Full Load Amp (FLA) which is calculated as (47).
The given motor shows the rated FLA is 5.8 A.
Assuming the PF of 0.82 we can also find the efficiency (48);

$$I_m = FLA = \frac{2 \times 746}{220 \times \text{Efficiency} \times 0.82 \times \sqrt{3}}\text{A} \qquad (47)$$

$$Efficiency = \frac{2 \times 746}{220 \times 0.82 \times 5.8 \times \sqrt{3}} = 0.823\% \quad (48)$$

Therefore, the input currents will be given by (49)

$$\begin{bmatrix} i_{g1} \\ i_{g2} \\ i_{g3} \end{bmatrix} = \begin{bmatrix} I_m\sin(\omega t) \\ I_m\sin\left(\omega t - \frac{2\pi}{3}\right) \\ I_m\sin\left(\omega t - \frac{4\pi}{3}\right) \end{bmatrix}$$

$$+1.1\pi \begin{bmatrix} \sin(100\pi t) - \sin(100\pi t) \\ -\sin\left(100\pi t - \frac{2\pi}{3}\right) + \sin\left(100\pi t - \frac{4\pi}{3}\right) \\ -\sin\left(100\pi t - \frac{4\pi}{3}\right) + \sin(100\pi t) \end{bmatrix}$$

$$-1.1\pi \begin{bmatrix} -\sin\left(100\pi t - \frac{4\pi}{3}\right) + \sin(100\pi t) \\ \sin\left(100\pi t - \frac{2\pi}{3}\right) - \sin(100\pi t) \\ -\sin\left(100\pi t - \frac{2\pi}{3}\right) + \sin\left(100\pi t - \frac{4\pi}{3}\right) \end{bmatrix}$$
$$(49)$$

6 Capacitors Switching to Network

A microcontroller is programmed in such way the inserted capacitors are removed or switched off from the network as the inrush currents reduces to the running current; they are switched on when it rises beyond the running current. As the magnitude of the inrush current depends on the switch-in angle on the voltage cycle [18], the switch must be inserted at minimum or at 0 degrees and described in (50):

$$v_a = v_m\cos(\omega t)$$
$$v_b = v_m\cos\left(\omega t - \frac{2\pi}{3}\right) \quad (50)$$
$$v_c = v_m\cos\left(\omega t - \frac{4\pi}{3}\right)$$

The switching of capacitors is done in the network when the voltage across the two phases (line voltage between phases) is equal to zero, this is as same as saying; at the time equal to the roots (zeros) of the input equation and the waveforms for $v_a - v_b$ shown on Figure 16.

7 Time Roots Equation Calculation

The calculation in (22) is to find the time the switches will be triggered to insert capacitor into the network. Besides switching the capacitors when the voltage between two phases crosses zero, the conditions for switching capacitors are (51):

$$v_a - v_b = 0 \qquad (51)$$

which yields (52):

$$v_m \cos\left(\omega t - \frac{2\pi}{3}\right) = 0 \qquad (52)$$

Considering the frequency $f = 50 Hz$ and the input voltage $v = 220V$, the switching time t of the capacitors into the network possibility between phase $a\&b, b\&c$ and $a \& c$ will can be calculated from (53).

$$v_m \cos(\omega t) - v_m \cos\left(\omega t - \frac{2\pi}{3}\right)$$
$$t = \frac{n}{100} - \frac{1}{150}, n \in Z \qquad (53)$$

$$v_a - v_c = 0 \qquad (54)$$
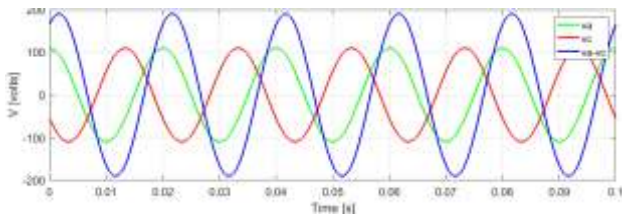
Fig. 16: Voltage va-vb plotting waveforms

$$v_m \cos(\omega t) - v_m \cos\left(\omega t - \frac{4\pi}{3}\right) \times$$
$$110\left(\cos(100\pi t) - \cos\left(100\pi t - \frac{4\pi}{3}\right)\right) = 0$$
$$t = \frac{n}{100} - \frac{1}{75}, n \in Z$$
$$(55)$$

Plotting the voltage $v_b - v_c$ and $v_a - v_c$ follows the same procedure as $v_a - v_b$. Since

$$v - vc = 0 \qquad (56)$$

$$v_m \cos\left(\omega t - \frac{2\pi}{3}\right) - v_m \cos\left(\omega t - \frac{4\pi}{3}\right) = 0 \quad (57)$$
$$v_m \cos\left(\omega t - \frac{2\pi}{3}\right) - v_m \cos\left(\omega t - \frac{4\pi}{3}\right) = 0$$
$$t = \frac{n}{100}, n \in Z \qquad (58)$$

Conditional roots which are the switching possibilities as given by the equations may be positive or negative values (practically, negative values of time are omitted, which is the condition given from the flowchart (Figure 17). Therefore, the circuit diagram for the system is given in Figure 18.

8   Prediction Results with Simulink
In the simulation, the inrush current of a 2 HP, 3-phase Induction Motor attains 65.71 A and starts

reducing after a delay of 5.5 s and maintains 5.8 A for the rest of the running time (Figure 19). The delay varies from one machine to another depending on their parameters with respect to the network. For the case of the considered machine also, the power factor is given in Figure 20.

Once the conditions are met for insertion of capacitors as discussed in Section III and also with the size of capacitor calculated from (21); the capacitors are inserted. The inrush current is reduced to 49.01 A which constitutes a 25.43 % reduction. The rotational speed and torque characteristics are the same as the DOL case, settling after 5.3 s to 1493 rpm as shown in Figure 21.

The comparison between currents with a DOL and the current system is shown in Figure 19 which illustrates the current reduction.
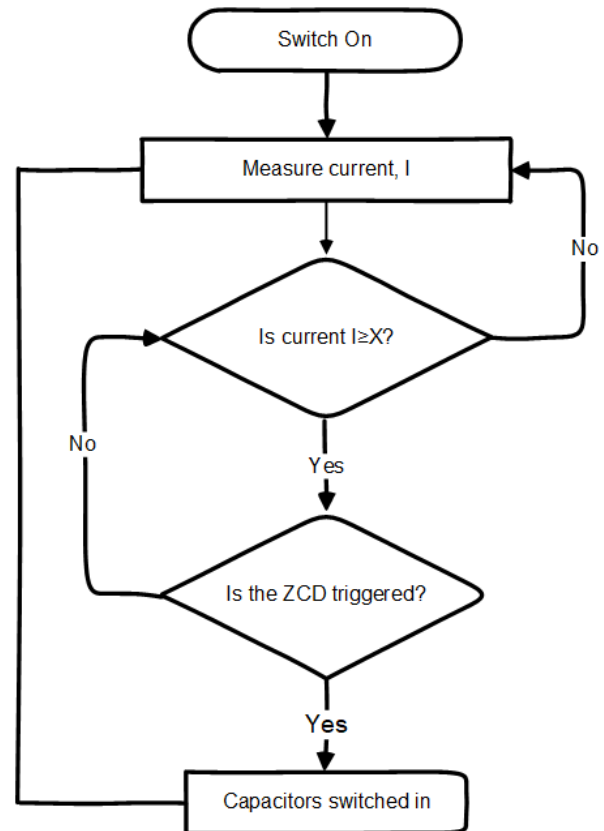
Fig. 17: Capacitor switching flowchart
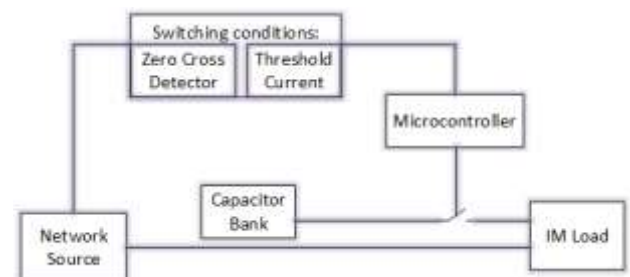
Fig. 18: Switching circuit diagram

9 Conclusion

As previously shown in a prior study, [12] which was simulation-based, it has been feasible to cut the beginning current by 50 % with the 5 HP, three-phase Induction motor by tweaking compensation capacitors.
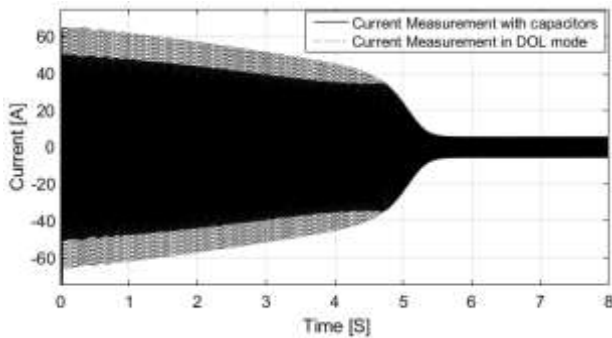
Fig. 19: Current measurements comparison
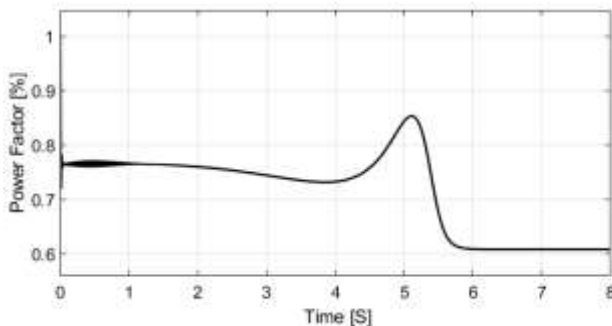
Fig. 20: Motor power factor

In this research, the results are obtained from a small 2 HP machine where the starting current is reduced by 25%. This may lead to the conclusion that the larger machines are used with the same research methodology. More research will be carried on with more scientific aspect involved in this scope.
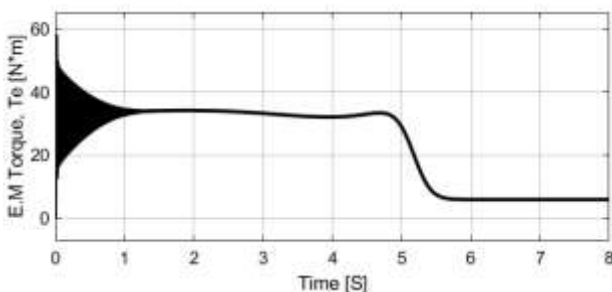
Fig. 21: Electromagnetic torque

Additionally, active power adjustment can be used to reduce current even further. However, this will require energy storage and an inverter, but the result will be more manageable. This will be the subject of future research as well.

In this research the implementation is aligned with the simulation: before connecting the control circuit to the physical load, a Speedgoat Real-time Simulator (the development tool

available in the lab) will be used to carry out Hardware In The Loop (HIL) testing before testing on a real system.

References:

[1]   H. Rehaoulia and M. Poloujadoff, "Transient behavior of the resultant airgap field during run-up of an induction motor," *IEEE Transactions on Energy Conversion,* no. 4, pp. 92-98, 1986.

[2]   E. Kurtz, "Transformer current and power inrushes under load," *Electrical Engineering,* vol. 56, no. 8, pp. 989-994, 1937.

[3]   C. Hayward, "Prolonged inrush currents with parallel transformers affect differential relaying," *Electrical Engineering,* vol. 60, no. 12, pp. 1096-1101, 1941.

[4]   M. Akherraz, "Inrush current and speed regulation of induction motor drives," in *[1991 Proceedings] 6th Mediterranean Electrotechnical Conference*, 1991: IEEE, pp. 1285-1288.

[5]   K. Pillay, M. Nour, K. Yang, D. D. Harun, and L. Haw, "Assessment and comparison of conventional motor starters and modern power electronic drives for induction motor starting characteristics," in *2009 IEEE Symposium on Industrial Electronics & Applications*, 2009, vol. 2: IEEE, pp. 584-589.

[6]   A. A. Shaltout, "Analysis of torsional torques in starting of large squirrel cage induction motors," *IEEE transactions on energy conversion,* vol. 9, no. 1, pp. 135-142, 1994.

[7]   N. Ragavendra, H. Suresh, J. Mohana Lakshmi, K. Shruthi, and T. Shruthi, "Fabrication and Development of Signal Loss Recovery System for AC Drives", *International Journal of Emerging Technology and Advanced Engineering*, Vol. 3, Issue 8, August 2013, pp.164-171.

[8]   L. Finzi and W. Mutschler, "The inrush of magnetizing current in single-phase transformers," *Transactions of the American Institute of Electrical Engineers,* vol. 70, no. 2, pp. 1436-1438, 1951.

[9]   P. Amiri and M. Akhbari, "Transient current limiter for suppressing transformer inrush,

motor starting and fault currents in power system," *IET Electric Power Applications,* vol. 11, no. 3, pp. 423-433, 2017.

[10] J. Larabee, B. Pellegrino, and B. Flick, "Induction motor starting methods and issues," in *Record of Conference Papers Industry Applications Society 52nd Annual Petroleum and Chemical Industry Conference*, 2005: IEEE, pp. 217-222.

[11] S. Chen, T. A. Lipo, and D. Fitzgerald, "Source of induction motor bearing currents caused by PWM inverters," *IEEE Transactions on Energy conversion,* vol. 11, no. 1, pp. 25-32, 1996.

[12] M. Habyarimana and D. Dorrell, "Methods to reduce the starting current of an induction motor," in *2017 IEEE International Conference on Power, Control, Signals and Instrumentation Engineering (ICPCSI)*, 2017: IEEE, pp. 34-38.

[13] M. Habyarimana, D. G. Dorrell, and R. Musumpuka, "Reduction of Starting Current in Large Induction Motors," *Energies,* vol. 15, no. 10, p. 3848, 2022.

[14] Valiadis Hellenic Motors. "OUR MOTORS", [Online]. https://www.valiadis.gr/?view=138 (Accessed Date: July 2, 2024).

[15] P. C. Sen, *Principles of Electric Machines and Power Electronics, International Adaptation*. John Wiley & Sons, 2021.

[16] S. Jain, J. Sharma, and S. Singh, "Transient performance of three-phase self-excited induction generator during balanced and unbalanced faults," *IEE Proceedings-Generation, Transmission and Distribution,* vol. 149, no. 1, pp. 50-57, 2002.

[17] C. Tindall and W. Monteith, "Balanced operation of 3-phase induction motors connected to single-phase supplies," in *Proceedings of the institution of Electrical Engineers*, 1976, vol. 123, no. 6: IET, pp. 517-522.

[18] I. Farzadfar, "*An inrush current model for core type transformers*," 1997, [Online]. https://www.nlc-bnc.ca/obj/s4/f2/dsk3/ftp05/mq23298.pdf (Accessed Date: July 2, 2024).